Pergamon

Int. J. Heat Mass Transfer. Vol. 37, No. 13, pp. 1867–1875, 1994

0017-9310/94 $7.00+0.00

0017-9310(94)E0017-O

Laminar flow and heat transfer from multiple impinging slot jets with an inclined confinement surface

S. H. SEYEDEIN, M. HASAN† and A. S. MUJUMDAR

Department of Chemical Engineering, McGill University, 3480 University St., Montreal, Quebec, Canada H3A 2A7

(*Received* 17 *May* 1993 *and in final form* 22 *December* 1993)

Abstract—Results of numerical simulation of two-dimensional flow field and heat transfer due to laminar heated multiple slot jets discharging normally into a converging confined channel are presented. A control volume-based finite difference method was employed to solve the governing mass, momentum and energy equations. To handle the complexity of the geometry a program was developed using a non-orthogonal body-fitted coordinate system. A fully staggered grid system was generated using the solution to a set of elliptic grid generation equations. The parameters studied were: the jet Reynolds number ($600 < Re < 1000$), and the angle of inclination of the upper surface ($0° < \theta < 20°$). Inclination of the confined surface so as to accelerate the exhaust flow was found to level the Nusselt number distribution on the impingement surface.

1. INTRODUCTION

SINGLE and multiple impinging jets find numerous industrial applications because of their highly attractive local heat and mass transfer characteristics. They range from annealing of non-ferrous metal sheets and glass, drying of paper, textiles, veneer, coated webs, etc. to cooling of microelectronic components. While many applications involve turbulent jets, laminar jets are also encountered when the fluid is very viscous (e.g. liquid), the gas temperature is high or the geometry is miniature (e.g. microelectronics). Numerous studies have been reported in the literature on the flow, heat and mass transfer distributions under single and multiple laminar impinging jets which are confined between two parallel plates, viz. the nozzle plate through which the jets issue and the impingement plate which is parallel to it. Effects of oblique impingement, transpiration through the wall, mass transfer at the target surface, cross-flow as well as motion of the target surface have been studied numerically. Polat *et al.* [1] have reviewed most of the relevant computational studies reported prior to 1989.

One of the limitations of impinging jets is the fact that they necessarily yield a highly non-uniform heat transfer rate distribution over the impingement surface. The highest Nusselt number occurs under the jet with much lower values in the wall jet region; this drop may be up to tenfold. Further, the spent flow from upstream jets deteriorates the thermal performance of the downstream jets—this is the so-called cross-flow effect.

Since Polat *et al.* [1] reviewed critically the relevant literature on the simulation of laminar confined impinging jets of various configurations subject to a wide variety of boundary conditions, no attempt will be made to repeat them here. Suffice it to say that almost all the prior work on laminar impinging jets deals with impingement on planar surfaces with either no confinement of the flow or with a confinement surface that is parallel to the impinged surface. The experimental studies of Schuh and Pattersson [2] and Marple *et al.* [3] indicate that the impingement flow is laminar in the whole domain of interest if the jet Reynolds number is under 1000. The effect of cross-flow which arises in the multiple impingement jet configurations was recently considered in the numerical work carried out by Al-Sanea [4]. As expected, he found that the presence of a cross-flow degrades the favourable heat transfer characteristics of impinging jets, and can reduce the nominal Nusselt number by as much as 60%. The studies closest to the configuration examined here are those due to Ichimiya and Hosaka [5] and Ichimiya [6]. They studied the impingement heat transfer characteristics of three confined slot jets experimentally (for laminar and turbulent jets) and numerically (for laminar case only). The laminar simulations were carried out for $Re = 500$. Both experimental and numerical results show the highly non-uniform Nusselt number distribution over the target surface with the peaks occurring just under or just downstream of the nozzle; the undesirable effect of spent flow from upstream jets was also shown clearly.

The objective of this work was to determine the feasibility of reducing the degree of non-uniformity in multi-jet impingement by simply inclining the confinement surface (Fig. 1) so as to accelerate the flow in the downstream direction. Of course, this can have

†Author to whom correspondence should be addressed.

NOMENCLATURE

a_P, a_{nb}, b coefficients in the discretized governing equations
c_p specific heat
F_x, F_y external force in u and v momentum equations
h convective heat transfer coefficient
J Jacobian of the transformation
K thermal conductivity
n normal direction
Nu_x local Nusselt number over the impingement surface
P pressure
ΔP pressure relative to the ambient pressure
ΔP_0 stagnation pressure relative to the ambient pressure
$\dot{q}''_s$ heat flux to impingement surface
Re_j jet Reynolds number
S centerline-to-centerline distance between two adjacent nozzles
S_Φ source term associated with Φ
T temperature
T_{conf}, T_{imp} temperature at the confinement and impingement surfaces
T_{in}, T_j inlet temperature
u, v velocity components in the x and y directions
U, V contravariant velocity components in ξ and η directions
$\tilde{v}_{in}$ inlet velocity
W nozzle width for slot jet
x, y corresponding to x and y directions in a Cartesian coordinate system.

Greek symbols
α, β, γ geometric relations between coordinate systems
$\alpha_p, \alpha_u, \alpha_v, \alpha_T$ under-relaxation factor for ΔP, u, v and T equations
Γ_Φ diffusion coefficient associated with Φ value
μ viscosity
Φ transported scalar
ρ mass density
θ inclination angle of confinement surface
ξ, η axes of non-orthogonal curvilinear coordinate system
$\Delta\xi, \Delta\eta$ length of the sides of control volume.

Subscripts
e, w, n, s four surfaces of control volume centered at P
E, W, N, S, NE, NW, SE, SW eight adjacent nodes to P
i, j indices for Cartesian components
P nodal point to be solved in difference equation
ξ, η, x, y partial derivatives with respect to ξ, η, x, y
Φ refers to dependent variables.

Superscripts
~ corrected values according to corrected pressure field.

a deleterious effect in increasing the cross-flow velocity seen by the downstream jets but a positive one in enhancing the heat transfer rate between adjacent jets. Also, since the downstream jets are closer to target surface this counteracts the effect of increased crossflow velocities. To handle the non-Cartesian boundary due to inclined confinement surface, the finite volume method due to Patankar [7] was modified and extended to a non-orthogonal boundary-fitted coordinate system. The equations and solution procedure are described briefly in the next section.

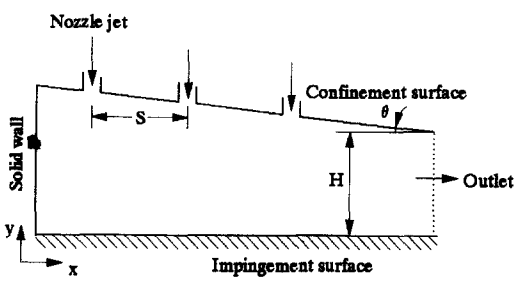

FIG. 1. The configuration of multiple impinging jets with inclined confinement surface.

2. MATHEMATICAL FORMULATION

In the present study a two-dimensional, steady-state laminar multiple jet impinging is considered as shown schematically in Fig. 1. The solid wall is considered as the boundary at the left side of the domain.

The two-dimensional conservation equations of mass, momentum and energy for a Newtonian fluid in steady laminar flow are:

Continuity:

$$\frac{\partial(\rho u_i)}{\partial x_i} = 0; \tag{1}$$

Momentum:

$$\frac{\partial(\rho u_i u_j)}{\partial x_i} = \frac{\partial}{\partial x_i}\left(\mu \frac{\partial u_j}{\partial x_i}\right) - \frac{\partial P}{\partial x_j} + F_j; \tag{2}$$

Energy equation:

$$\frac{\partial(\rho c_p u_i T)}{\partial x_i} = \frac{\partial}{\partial x_i}\left(k\frac{\partial T}{\partial x_i}\right) + S_T \quad (3)$$

Here F_j is any external force which acts directly on the mass of the fluid; S_T is the rate of generation or dissipation of energy.

A combination of the control volume-based finite difference method with body-fitted coordinate system was used to solve the governing equations. With a boundary-fitted coordinate (BFC) system the domain boundaries coincide with coordinate lines and allow boundary conditions to be applied directly without interpolation, resulting in enhanced accuracy.

The first step in using the BFC technique is to find the nodal points which are influenced by the boundaries; these can be obtained from a suitable grid generation technique. In a grid generation technique every nodal point in the physical domain coincides with a corresponding node in the computational domain. In the present study, this mapping of physical domain to computational domain is provided by a set of elliptic PDEs in the form of the Laplace equations as follows, Thompson [8]:

$$\xi_{xx} + \xi_{yy} = 0, \quad (4)$$

$$\eta_{xx} + \eta_{yy} = 0, \quad (5)$$

where ξ and η represent the coordinates in the computational domain. The inverse transformation of the Laplace equations yields:

$$\alpha x_{\xi\xi} - 2\beta x_{\xi\eta} + \gamma x_{\eta\eta} = 0, \quad (6)$$

$$\alpha y_{\xi\xi} - 2\beta y_{\xi\eta} + \gamma y_{\eta\eta} = 0, \quad (7)$$

where

$$\alpha = x_\eta^2 + y_\eta^2, \quad (8)$$

$$\beta = x_\xi x_\eta + y_\xi y_\eta, \quad (9)$$

and

$$\gamma = x_\xi^2 + y_\xi^2. \quad (10)$$

Depending on the orthogonality of the faces of the control volume cells, a boundary fitted coordinate system can be either orthogonal or non-orthogonal. In this work, the coordinate system was chosen to be non-orthogonal and the problem was solved in the transformed domain using the physical Cartesian velocity components.

2.1. *Transformation of governing equations*

The general form of transformed governing equations becomes:

$$\frac{\partial(\rho U\Phi)}{\partial\xi} + \frac{\partial(\rho V\Phi)}{\partial\eta} = \frac{\partial}{\partial\xi}\left[\mu\left(\frac{\alpha}{J}\frac{\partial\Phi}{\partial\xi} - \frac{\beta}{J}\frac{\partial\Phi}{\partial\eta}\right)\right] + \frac{\partial}{\partial\eta}\left[\mu\left(\frac{\gamma}{J}\frac{\partial\Phi}{\partial\eta} - \frac{\beta}{J}\frac{\partial\Phi}{\partial\xi}\right)\right] + S_\Phi(\xi,\eta), \quad (11)$$

where the Jacobian of transformation J, and contravariant velocity components U and V are:

$$J = x_\xi y_\eta - y_\xi x_\eta, \quad (12)$$

$$U = uy_\eta - vx_\eta, \quad (13)$$

and

$$V = vx_\xi - uy_\xi. \quad (14)$$

The value of Φ and the associated definitions of Γ_Φ and S_Φ for the governing equations are:

Continuity:

$$\Phi = 1, \quad \Gamma_\Phi = 0, \quad S_\Phi = 0,$$

x-Momentum:

$$\Phi = u, \quad \Gamma_\Phi = \mu, \quad S_\Phi = -y_\eta\frac{\partial P}{\partial\xi} + y_\xi\frac{\partial P}{\partial\eta},$$

y-Momentum:

$$\Phi = v, \quad \Gamma_\Phi = \mu, \quad S_\Phi = -x_\xi\frac{\partial P}{\partial\eta} + x_\eta\frac{\partial P}{\partial\xi},$$

Energy:

$$\Phi = T, \quad \Gamma_\Phi = \frac{k}{c_p}, \quad S_\Phi = 0.$$

2.2. *Discretization of governing equations*

The governing transport equations, equation (11), along with the boundary conditions were discretized according to the staggered-grid control volume finite-difference approach. In this approach all the scalar variables are computed at the geometric centers of the control volumes while the Cartesian and contravariant velocity components are calculated at the centers of the faces of the control volumes in the (ξ, η) plane. In the discretization of the momentum equations the method due to Shyy *et al.* [9] was used.

Applying a staggered-grid system to discretize the governing momentum equations we obtain:

$$a_e u_e = \sum_{nb} a_{nb} u_{nb} + b_e^u - \left[\left(P_E - P_P\right)y_\eta^e - \frac{P_N + P_{NE} - P_S - P_{SE}}{4}y_\xi^e\right], \quad (15)$$

$$a_e v_e = \sum_{nb} a_{nb} v_{nb} + b_e^v - \left[\frac{P_N + P_{NE} - P_S - P_{SE}}{4}x_\xi^e - \left(P_E - P_P\right)x_\eta^e\right]. \quad (16)$$

The coefficients a_e and a_{nb} are the same in both equations while b_e^u and b_e^v are the cross-derivative source terms given by:

$$b_c^u = -\left(\frac{\beta}{J}\Gamma\right)_e \frac{u_N + u_{NE} - u_S - u_{SE}}{4} + \left(\frac{\beta}{J}\Gamma\right)_w \frac{u_N + u_{NW} - u_S - u_{SW}}{4} - \left(\frac{\beta}{J}\Gamma\right)_n \frac{u_E + u_{NE} - u_W - u_{NW}}{4} + \left(\frac{\beta}{J}\Gamma\right)_s \frac{u_E + u_{SE} - u_W - u_{SW}}{4}, \quad (17)$$

$$b_c^v = -\left(\frac{\beta}{J}\Gamma\right)_e \frac{v_N + v_{NE} - v_S - v_{SE}}{4} + \left(\frac{\beta}{J}\Gamma\right)_w \frac{v_N + v_{NW} - v_S - v_{SW}}{4} - \left(\frac{\beta}{J}\Gamma\right)_n \frac{v_E + v_{NE} - v_W - v_{NW}}{4} + \left(\frac{\beta}{J}\Gamma\right)_s \frac{v_E + v_{SE} - v_W - v_{SW}}{4}. \quad (18)$$

The metric derivatives, i.e. x_ξ, x_η, y_ξ and y_η are calculated directly at the control volume surfaces which conforms with the physical conservation laws more accurately, Shyy *et al.* [9].

2.3. *Derivation of pressure correction equation*

In the SIMPLE algorithm the pressure correction equation is specified indirectly via the discretized continuity equation. The general form of the pressure correction in the body-fitted coordinates system includes eight neighbour points as follows:

$$a_P \tilde{P}_P = a_E \tilde{P}_E + a_W \tilde{P}_W + a_N \tilde{P}_N + a_S \tilde{P}_S + a_{NE} \tilde{P}_{NE} + a_{NW} \tilde{P}_{NW} + a_{SE} \tilde{P}_{SE} + a_{SW} \tilde{P}_{SW} + B. \quad (19)$$

Since the successive line-by-line method was used to solve the system of algebraic equations, the terms involving $\tilde{P}_{NE}$, $\tilde{P}_{SE}$, $\tilde{P}_{NW}$ and $\tilde{P}_{SW}$ in the pressure correction equation was dropped for the sake of simplicity and computational flexibility. For a detailed description of the discretization of the governing transport equations along with the expressions for the 'a' coefficients the reader is referred to Seyedein [10].

2.4. *Boundary conditions*

Solid wall boundary conditions. Along the solid walls, the no-slip boundary condition for velocities and known values for temperature were used as follows:

$$u|_{wall} = v|_{wall} = U|_{wall} = V|_{wall} = 0$$

$$T_{conf} = T_{in} = 50°C \quad T_{imp} = 25°C \quad T_w = 50°C.$$

The temperatures chosen have applications in impingement drying.

The discretized form of the u-momentum equation in the non-orthogonal body-fitted coordinate system includes pressure gradient at location 'e'. The pressure gradient at this location for the north or south boundaries can be found from a backward or a forward difference scheme, respectively. For the boundary position along with the grid points shown in Fig. 2 it becomes:

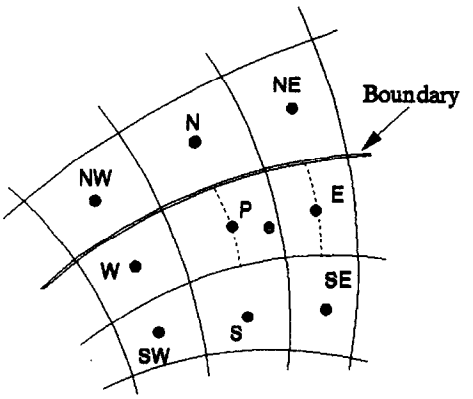

FIG. 2. Control volume for u-velocity at the boundary in the physical domain.

$$\left.\frac{\partial P}{\partial \xi}\right|_e = P_E - P_P,$$

$$\left.\frac{\partial P}{\partial \eta}\right|_e = \frac{(P_E - P_{SE}) + (P_P - P_S)}{2}$$

(using backward difference).

Outlet boundary conditions. The flow and temperature at the outlet surface in the physical domain were assumed to be fully developed. The transformation of this boundary condition from the physical domain to the computational domain results in

$$\alpha \frac{\partial \Phi}{\partial \xi} - \beta \frac{\partial \Phi}{\partial \eta} = 0, \quad \text{where } \Phi \text{ represents } u, v \text{ or } T.$$

Nozzle exit boundary conditions. The uniform velocity and temperature profiles were assumed at the nozzle exit:

$$u = 0 \quad v = v_{in} \quad T = T_{in} = 50°C.$$

2.5. *Numerical solution*

The numerical solution procedure is based on Patankar's SIMPLE algorithm [7]. The velocity component u is calculated at the east and west faces of the main control volumes from the solution of the u-momentum equation. Then, the same velocity component at other faces is obtained by interpolation. Similarly, velocity component v at the control volume faces is obtained. In each iteration the contravariant velocity components U and V are calculated just after any changes in the physical velocity field. The contravariant velocity components as well as pressure are corrected based on the recently obtained ΔP from solution of the pressure correction equation. For the new iteration the physical velocity components are

calculated using the corrected contravariant velocity components. This iteration loop is terminated if the maximum absolute residual (normalized by the corresponding fluxes at the nozzle exit) of the discretized equations approaches a small value, the so-called convergence criterion.

The convergence criterion for most runs was chosen to be 0.005 but to estimate the degree of accuracy runs with convergence criteria as low as 0.001 were also carried out. The difference between the predicted Nusselt number profiles obtained using these criteria were found to be under 0.1%. Thus, most runs were performed with $CC = 0.005$ to save computational time.

To obtain grid independent results two different grid distributions i.e. 42×42 and 54×54, were tested. The maximum difference in the results of local Nu was 3.5%. Again, for the sake of computational economy most runs were performed with the 42×42 grid layout.

Effect of under-relaxation and stability. In the present study much effort was devoted to find the appropriate under-relaxation factors. Various combinations of under-relaxation factors were examined and after numerous runs the following set was selected for the production runs:

$$\alpha_u = 0.6 \quad \alpha_v = 0.6$$

$$\alpha_p = 0.02 \quad \alpha_T = 0.7.$$

The stability of the computation depends on the type of interpolation scheme used for the approximation of Φ at the control volume surfaces. To consider the effect of the interpolation scheme used, two different schemes, i.e. hybrid and upwind schemes, were tested. For the case with the inclination angle of the confinement surface equal to 20°, the simulation using the hybrid scheme was found to be unstable while a similar run was successfully performed using the upwind scheme. For confinement surface inclination angles of less than 20° stable runs were obtained using both schemes. No explanation can be offered for this observation due to the limited effort devoted to this aspect.

The program was coded in MS-DOS FORTRAN 77 and executed on a 33 MHz PC386 with an Intel 80387 co-processor. An NDP20 compiler was used to compile the program. The computer time required was about 3.03 CPU seconds per iteration.

3. RESULTS AND DISCUSSION

Since experimental data on flow and heat transfer for laminar impinging jets with inclined confinement surface have not been documented in the literature, the code developed in the present work was validated on the basis of validated programs written in the Cartesian system for the standard non-inclined confinement case. Also good agreement with the experimental data reported in the literature was observed

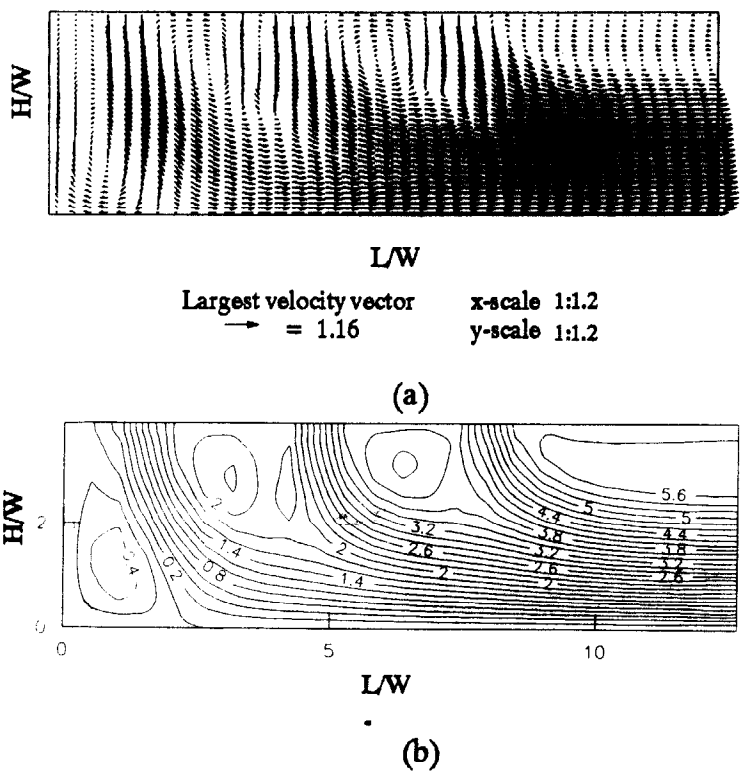

FIG. 3. Vector plots (a), and streamline contours (b), for multiple laminar impinging jets with inclined confinement surface, $Re = 800$, $\theta = 0°$.

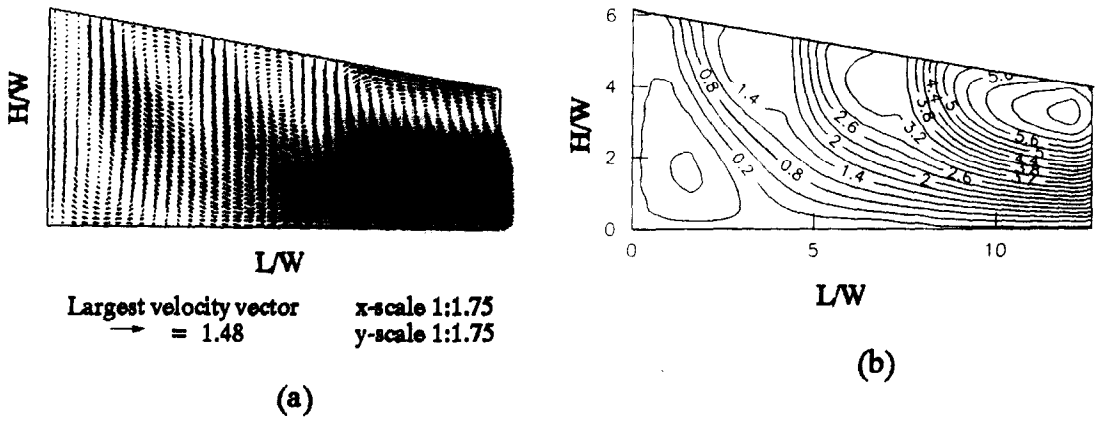

FIG. 4. Vector plots (a), and streamline contours (b), for multiple laminar impinging jets with inclined confinement surface, $Re = 800$, $\theta = 10°$.

for the case of single jets and parallel confinement surface.

3.1. *Flow patterns*

The calculated velocity vector plots and streamline contours for $Re = 800$, H/W at exit equal to 4, $S/W = 3.334$ and different angles of inclination are shown in Figs. 3–5. Since a solid wall boundary has been used on the left boundary, the flow turns towards the outlet at the right-hand boundary. This arrangement of jets results in a deflection of individual jets in the downstream direction and a shift of the corresponding stagnation lines. The recirculation zone behind the first jet from the left is due to the space between the first jet and left solid wall. In this region, the lateral velocity along the impingement surface is negative and, at the corner, the x-direction velocity changes to the y-direction velocity and behaves as a weak impinging jet for the left solid wall. Downstream of each of the three successive jets, a recirculation zone develops. The size of each one of these recirculation zones diminishes with increase of the axial distance from the left wall to the outlet. This behavior is due to the combined effect of the reduction in the cross-sectional area between the confinement and impingement surfaces and the increase in the cumulative flow due to the upstream jets.

Although inflow from the outlet boundary influences the computation of the recirculation zones, according to van Heiningen [11], its effect on the local heat transfer distribution over the impingement surface is small. In the present study, in which heat transfer is of major concern, the length of the domain was chosen to be 13 times the width nozzle, although this allowed a certain amount of inflow at the downstream boundary.

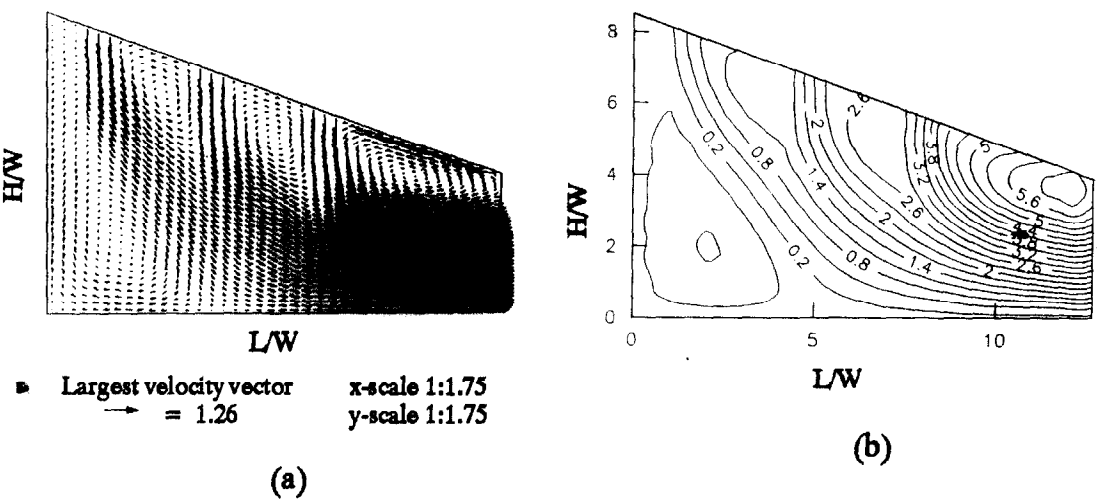

FIG. 5. Vector plots (a), and streamline contours (b), for multiple laminar impinging jets with inclined confinement surface, $Re = 800$, $\theta = 20°$.

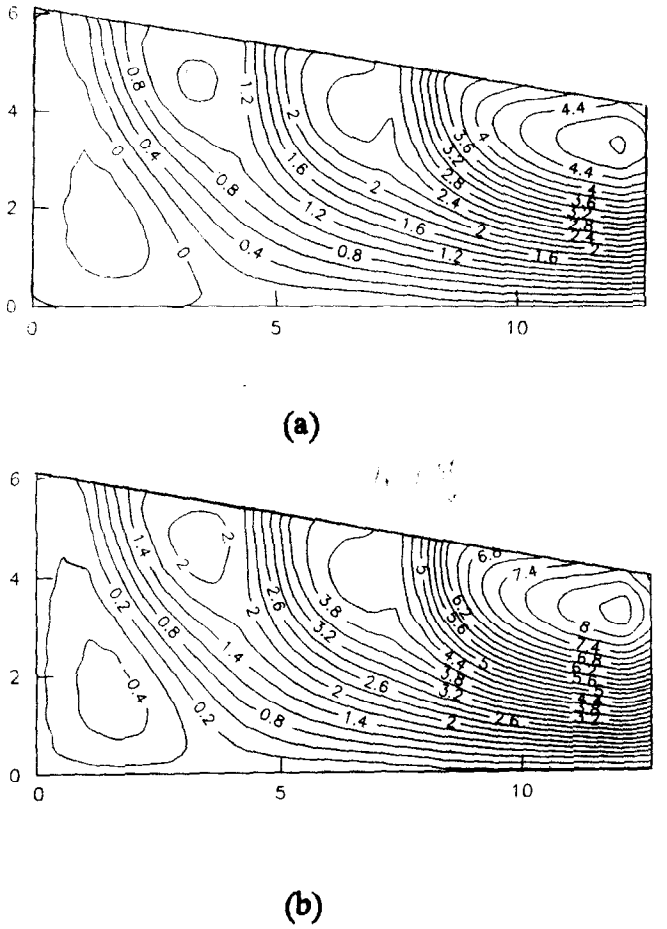

FIG. 6. Effect of Reynolds number on the recirculation zones for multiple laminar impinging jets with inclined confinement surface, $\theta = 10°$, (a) $Re = 600$; (b) $Re = 1000$.

It is noted that the jet Reynolds number has little effect on the size of the recirculation region (Fig. 6) while increasing θ enlarges the size of these regions (Fig. 4).

3.2. *Static pressure distribution along impingement surface*

Static pressure along the impingement surface was normalized as $\Delta P/\Delta P_0$, where ΔP is pressure along

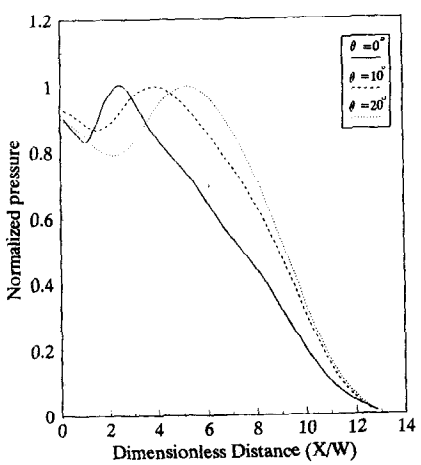

FIG. 7. Effect of the inclination angle on the static pressure distribution along the impingement surface.

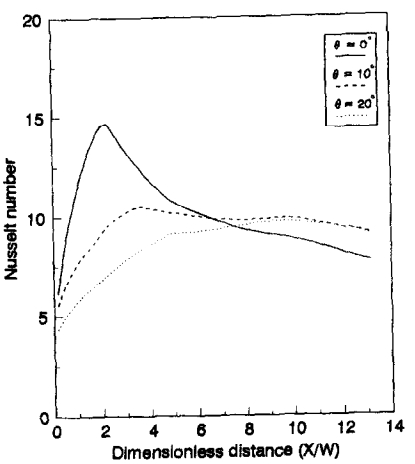

FIG. 8. Effect of the inclination angle of the upper confinement surface on the local Nu distribution along the impingement surface, for $Re = 800$ and $H/W = 4$.

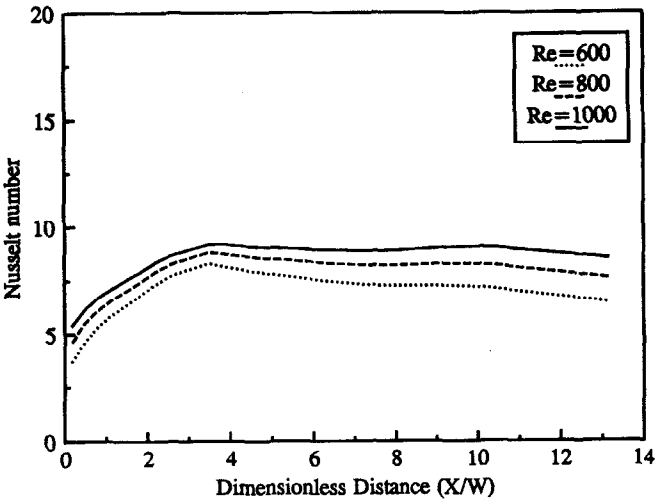

(a)

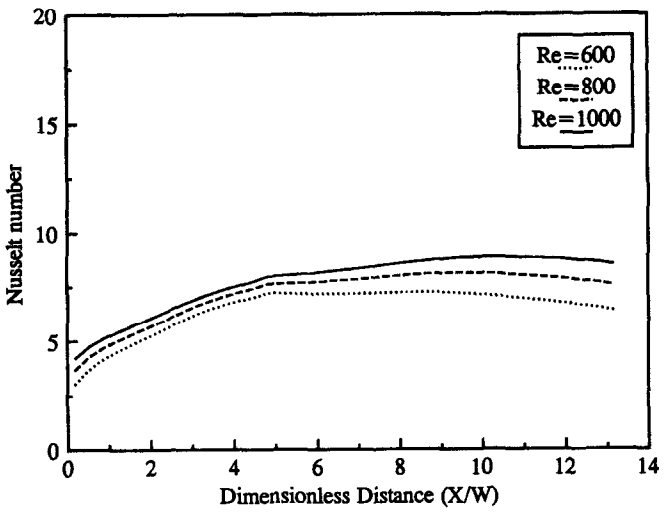

(b)

FIG. 9. Effect of Reynolds number and inclination angle of upper confinement surface on Nu distribution along the impingement surface, for $H/W = 4$, (a) $\theta = 10°$; (b) $\theta = 20°$.

the impingement surface relative to the ambient pressure and ΔP_0 is the stagnation pressure relative to the ambient pressure.

Figure 7 shows the variation of the normalized static pressure along the impingement surface at a Reynolds number of 800 and at different inclination angles. There are two maxima in these profiles which are attributed to the existence of two stagnation points, viz. one at the corner ($x = 0$) and the second at the location where the first jet impinges the surface. The second peak in static pressure, which represents a stagnation point over the impingement surface, moves towards the outlet as the inclination angle is increased. This movement is due to the acceleration of the exhaust flow caused by the reduction in the channel cross section in the downstream direction.

3.3. *Heat transfer results*

The local Nusselt number, Nu_x, is defined as:

$$Nu_x = \frac{h_x W}{k}, \quad \text{where } h_x = \frac{q_{w_x}}{T_{imp} - T_j}.$$

Figure 8 shows the variation of Nu_x along the impingement surface for $Re = 800$ and three different inclination angles of the confinement surface. For $\theta = 0°$, Nu_x first increases to its highest value at the stagnation point and then decreases rapidly downstream. The rate of Nusselt number reduction changes around $X = 5$ and $X = 8$, viz. under the second and the third jets, respectively. By increasing the inclination angle the variation of the Nu distribution between the first and the two downstream jets decreases. The maximum

in the Nu_x profile is seen to shift downstream with increase of θ. A comparison of the predicted Nu_x profiles for $\theta = 0°$, $10°$ and $20°$ shown in Fig. 8 shows that the maximum in Nu_x decreases with increasing θ. Further, the most uniform profile is obtained at $\theta = 10°$. Comparing these results with those for parallel confinement and impingement surfaces ($\theta = 0°$), the inclined confinement surface case has a higher value of Nu_x in the vicinity of the outlet. This once again is a result of the acceleration of the flow due to the reduction in cross-section in this region.

Figure 9 shows the effect of the jet Reynolds number on the predicted Nu_x distribution for $\theta = 10°$ and $20°$. As expected, increasing the Reynolds number causes the entire Nusselt number profile to shift to a higher value. The Nu_x distribution remains nearly uniform (if one neglects the region between the upstream wall and the first jet) while the 'imprints' of the second and third jets are hardly discernible. The non-uniformity in Nu_x distribution due to the presence of the upstream wall, however, cannot be adjusted by changing the angle of inclination or individual jet Reynolds number. The first jet will have to be directed towards the corner to raise the local heat transfer in this region. It should be noted that uniformity of the heat transfer distribution could also be controlled by changing the Reynolds numbers of successive jets. This case was not examined in the present study.

4. CONCLUDING REMARKS

The main conclusions obtained from the present study can be summarized as follows:

(1) A body-fitted transformation technique is a viable approach for the simulation of impinging jets in complex geometries. The transformed governing equations can be discretized over the computational domain in the same way as that for Cartesian coordinates. The resulting algebraic equations can be solved using the well-known tri-diagonal matrix algorithm (TDMA).

(2) Comparison of the predicted local Nusselt number profiles for a set of laminar impinging jets with an inclined confinement surface for different inclination angles (θ) showed that the inclination has a levelling effect on the Nu_x distribution over the impingement surface. By increasing the inclination angle (so as to accelerate the cross-flow) the maximum in the Nu_x profile decreases while the value of Nu_x downstream increases. The maximum in the Nu_x profile decreases with increase of θ; a high degree of uniformity in Nu_x profile is obtained with $\theta = 10°$. The levelling influence of inclination of the confining surface is also dependent on the jet Reynolds number, spacing between the two walls as well as inter-jet spacing.

Acknowledgements—The financial support provided by the Ministry of Culture and Higher Education of the Islamic Republic of Iran for this study is acknowledged. This research was supported by the National Science and Engineering Research Council of Canada.

REFERENCES

1. S. Polat, B. Huang, A. S. Mujumdar and W. J. M. Douglas. In *Annual Review of Numerical Fluid Mechanics and Heat Transfer* (Edited by C. L. Tien and T. C. Chawla), Vol. II, pp. 157–197. Hemisphere Publishing (1989).
2. H. Schuh and R. Pattersson, Heat transfer by arrays of two-dimensional jets directed normal to surfaces including the effects of superimposed wall parallel flow, *Flow Proc. 3rd Int. Heat Transfer Conf.* **2,** 280 (1966).
3. V. A. Marple, B. Y. H. Liu and K. T. Whitby, On the flow fields of inertial impactors, *J. Fluids Engng, Trans. of ASME, Series* I **96,** 394–400 (1974).
4. S. Al-Sanea, A numerical study of the flow and heat transfer characteristics of an impinging laminar slot-jet including crossflow effects, *Int. J. Heat Mass Transfer* **35,** 2501–2513 (1992).
5. K. Ichimiya and N. Hosaka, Experimental study of heat transfer characteristics due to confined impinging two dimensional jets (heat transfer experiment for three slot jets), *Trans. Japan Society of Mech. Engrs, B* **55,** 3210–3215 (1989).
6. K. Ichimiya, Numerical estimation on impingement heat transfer caused by confined three slot jets. In *Transport Phenomena in Heat and Mass Transfer* (Edited by J. A. Reizes), pp. 456–467. Elsevier Science (1992).
7. S. V. Patankar, *Numerical Heat Transfer and Fluid Flow*. Hemisphere Publishing (1980).
8. J. F. Thompson, Z. U. A. Warse and C. W. Mastin, *Numerical Grid Generation Foundations and Applications*. North-Holland (1985).
9. W. Shyy, S. S. Tong, and S. M. Correa, Numerical recirculating flow calculation using a body-fitted coordinate system, *Numerical Heat Transfer* **8,** 99–113 (1985).
10. S. H. Seyedein, Simulation of fluid flow and heat transfer in impingement flow of various configurations, M.Sc. Thesis, Chem. Eng. Dept., McGill University (1993).
11. A. R. P. van Heiningen, Heat transfer under an impinging slot jet, Ph.D. Thesis, Dept. of Chem. Eng., McGill University (1982).